

Design and control of a multiple-section continuum robot with a hybrid sensing system

Yihua. Fang, Xin. Dong*, Abd Mohammad, Dragos Axinte

Abstract— After decades of development, the technology of continuum robots continues to mature gradually and is used for various applications, e.g., inspection and repair in high-value-added industries such as aerospace & nuclear. However, such robots are invariably designed with a hyper-redundant structure which causes condition-dependent uncertainties and errors in practical operations. In this work, a hybrid sensing solution - consisting of a dual displacement sensor system (linear & rotary encoders) and a self-carried visual tracking system - is presented to improve the control performance of a multi-section cable-driven continuum robot. The dual displacement sensor system works to measure the cable-displacement error at the proximal end of the arm and predicts the cable elongation in the arm to eliminate the control error of the robot in joint-space via a new two-stage cable-displacement control approach. Simultaneously, the self-carried visual system provides real-time section-by-section tip tracking to improve the controllability of the arm in the task space. This feedback is then integrated with a two-level closed-loop controller to achieve accurate tip-positioning control. A series of validation experiments are carried out to validate the approach. Compared with an off-the-shelf position tracking system (VICON), the measurement error of the proposed self-carried visual tracking system is smaller than 2 mm, with a mean error of 0.67 mm, within the work-space of a single-section continuum robot. The distal-tip control accuracy of a 2-section robot can achieve 1.72 mm under the closed-loop controller supported by the hybrid sensing system.

Index Terms— continuum robot, closed-loop control, visual tracking, tip-positioning.

I. INTRODUCTION

CABLE-DRIVEN continuum robots are a family of hyper-redundant robotic manipulators. This characteristic feature leads to several condition-dependent uncertainties and errors in practical systems. Consequently, the conventional theoretical kinematic or dynamic model controller introduces non-negligible errors in motion control. To account for this, adding sensors and developing new controllers could be the solutions to minimize the uncertainties and errors and improve the controllability of continuum robots. The control of the continuum robot can be classified into four operating spaces: actuation space, joint-space, configuration space, and task space¹ [1]. Various approaches have been developed to measure these robot parameters and provide feasible feedback to achieve closed-loop control of the arm. Generally, the sensing methods can be

divided into two categories: contact and contactless.

Contact sensing methods usually pertain to built-in sensors. For example, displacement sensors such as string potentiometers (metallic cables) and linear or rotary encoders are always employed in continuum robot system, to improve control accuracy in joint-space or estimate robot configuration. These sensors are commonly mounted in the actuation pack or the arm structure to measure tendon displacement and arm elongation, restoring arm shape and tip position with the kinematics models [2-5]. However, this indirect shape estimation has inherent errors introduced by mismatches between the theoretical model and the actual arm shape [6]. In more general cases, embedded sensors, such as FBG (Fiber Bragg Grating) sensors, can directly rebuild the robot shape by integrating detected local elongation (strain) along with the arm structure. This type of sensing system is more expensive than the other commercial ones, which is a hurdle for FBGs usage in extreme applications (e.g., high temperature and radiation) [7]. In contrast, flex bending sensors and strain gauges are affordable alternative solutions. The former provides segment curvature measurement, and the latter detects local deflection [8, 9]; neither measurement is as accurate as FBGs and they are not suitable for shape sensing in slender arms as errors accumulate along the length.

On the other hand, contactless shape sensing and tip tracking rely on external measurement devices. Magnetic trackers are commonly used in small-scale operations [10]. These systems consist of several magnetic sensors attached to the tips of the sections of the arm and a processor tracking the sensors in an artificial magnetic field generated by a transmitter. Both position and orientation measurements are provided at high accuracy, based on the magnetic field variation, with a position error of 1.4 mm RMS and an orientation error of 0.5°RMS [11]. However, it is limited by its working principle, as any ferromagnetic material in the robot or near field can significantly influence the precision of the measurement. In contrast, external vision systems are more feasible for larger-scale applications. This type of measurement system can be configured by infrared cameras [3], depth cameras, or even general webcams [12], requiring multi-camera views from known positions in the work-space. After calibrating the camera array, the position and orientation of an object marker can be obtained. Overall, the external measurement methods can capture robot shapes precisely, eliminating the error in

* This research was funded by the Aerospace Technology Institute (UK) under Grant Agreement No. 104823 (CHIMERA – Robotic Inspection of Pressure Vessels). (Corresponding author: Xin Dong.)

Y. Fang, X. Dong, Abd Mohammad, D. Axinte are with the Department of Mechanical, Materials and Manufacturing Engineering, University of Nottingham, Nottingham NG7 2RD, U.K. (e-mail: {Yihua.Fang, Xin.Dong, Abd.Mohammad1, Dragos.Axinte}@nottingham.ac.uk).

¹ For a cable-driven continuum robot, the actuation space and joint space control refer to the actuation motor and actuation cables respectively. The configuration space indicates the robot arm arc parameters such as bending angle (θ) and direction angle (ϕ) of each section. The task space refers to position, orientation, and force control of the robot tip in the global coordinate.

calculation compared to contact sensing. However, it is difficult to implement in confined spaces since the view of the cameras would be blocked by obstacles.

With the development of sensing devices, various intelligent controllers were developed. The conventional model-based controller depends highly on accurate modeling, either for static or dynamic control in configuration space [1, 13]. Nevertheless, the inherent characteristics of continuum robots make it challenging to establish a precision model to predict potential errors under variant working conditions. Recent research focuses on closed-loop control to solve these problems, especially by using model-less or model-free methods. The closed-loop controllers can be classified based on operating spaces [1, 14]. Joint to configuration space controllers typically rely on sensors measuring the displacement of the actuation to eliminate the input control error (i.e., actuation cables, steel strings, etc.). This type of controller is usually based on PID control or integrated with non-linear methods such as neural networks [15, 16]. There remain unsolved problems regarding the cable elongation within the robot structure and the condition-dependent modeling error, bringing control uncertainty in configuration and task space.

In comparison, task-space closed-loop controllers work in positioning the robot tip in 2-D or 3-D work-space directly, while configuration-space controllers control the robot tip indirectly. Conventionally, inverse kinematics or dynamic models are established for a continuum robot to convert Cartesian tip movement to actuation tendon displacement [17]. In recent years, model-less or model-free methods have increasingly attracted attention to reduce the dependency on modeling and improve the adaptivity of a robot under different working scenarios. For instance, the practice of online learning can help obtain an instant inverse mapping between the actuation and end-effector to predict the non-linear and time-varying model of continuum robots [18]. Another example is to build an empirical map from the task space to the actuation one based on the fuzzy logic algorithm to converge tip errors stably and efficiently in the closed-loop process [6].

In summary, feedback systems and controller design are two key elements contributing to the control accuracy of continuum robots. This paper proposes a hybrid sensing system that is able not only to compensate for the tendons' displacement uncertainties (e.g., elongation, positioning on the spool winding system) but also to minimize the coupling effect between the sections of the continuum robot (a major problem in multi-segmented snake robots). This sensing system is distributed along the continuum arm: (i) for the coupling effect, a self-carried visual tracking system formed by several paired observe-reference camera & marker arrays are mounted at the base of each section to correct the pose of the arm; (ii) to improve the cable displacement control accuracy, a dual displacement sensor system (consists of linear & rotary sensors) is embedded to measure the displacement error within actuation pack and predict the elongation in the arm structure. Equipped with this comprehensive sensing system and a novel closed-loop controller, the continuum robot (two-section) can reduce the distal tip control error by 73.5% compared with conventional methods (Table 3), for both smooth and sharp movements. The paper is structured as follows: Section II

discusses the challenges in continuum robot control and briefly presents the design concept of the hybrid sensing system using dual displacement sensors in the actuation and camera arrays carried on the continuum arm. Section III introduces the hardware design of the integration and the two-level closed-loop controller based on the hybrid sensing system. Finally, in Section IV, a series of experiments were conducted to validate the proposed system and controller on a two-section cable-driven continuum robot, which demonstrates the accurate tip-positioning performance. Section V concludes this paper and gives some advice for further research work.

II. SENSING CHALLENGES OF CONTINUUM ROBOT AND THE NEW CONCEPT OF THE HYBRID SENSING APPROACH

In the field of tendon-driven continuum robotics, there are two main approaches for driving the actuation cables, which use linear or rotary actuation units. Rotary actuators can remarkably reduce the volume of the actuation system in comparison to linear actuators [19, 20], but pose a challenge for the control and modeling of continuum robots.

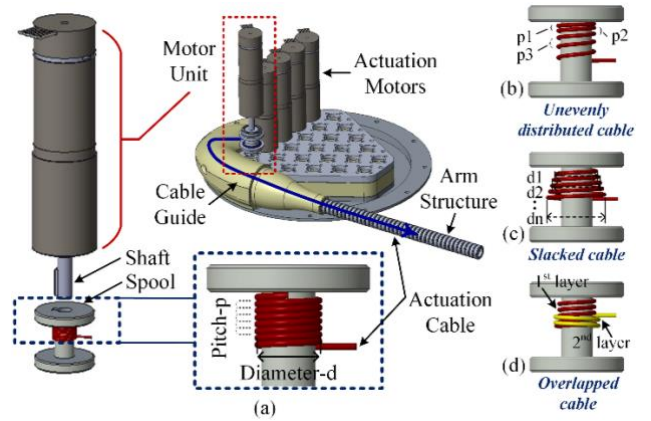


Fig. 1 Spool-driving actuation system for continuum robot with several uncertain practical cable windings scenarios. (a) Robot prototype with rotary (motor-spool) actuation and the ideal winding of the cable (constant pitch p and diameter d along the full length of the cable). (b) Uneven cable winding with unequal pitches ($p_1 \neq p_2$). (c) Slacked cable with unequal diameters ($d_1 \neq d_2$). (d) Overlapped cables with unequal diameters and increased friction.

Generally, for a rotary actuated continuum robot, a spool system is enrolled to connect to the rotary motor with a cable attached and coiled on it for a rotary actuation unit (Fig. 1a). There are two primary error sources for the joint-space cable-displacement estimation: 1) the incorrect conversion between the motor rotation and cable linear movement caused by the uncertain practical cable windings (Fig. 1b-d); 2) the cable elongation raised by the applied force along it. In an ideal situation, the cable is fully tensioned and winding on the spool with a constant pitch(p) and diameter(d) for each revolution (Fig. 1a). The relation between the motor rotation and the cable displacement is defined by $\Delta l = \frac{\omega_m}{2\pi} * \sqrt{p^2 + (\pi * d)^2}$, where Δl is the cable displacement and ω_m is the motor rotation angle. This calculation can theoretically predict the cable displacement based on the motor rotation measured by the rotary encoder, provided that the cable is properly tensioned, and the pitch is constant between the adjacent revolutions.

However, various practical issues can happen in the spool system, such as uneven cable distribution, cable slacking, overlapping, etc. (Fig. 1 b-d). These issues cannot be easily monitored by the existing sensing approaches, making the theoretical calculation invalid and posing a significant challenge to the modelling of the cable displacement, and affecting the positional accuracy of a continuum robot.

Furthermore, cable elongation exists along the entire length of the cable in both the actuation system and the continuum arm, which can primarily affect the prediction of the cable displacement and the control of the robot. The inhomogeneous time-varying friction distribution along the cable further challenges elongation modeling. The friction distribution is affected by various factors, such as the shape of the arm, initial cable tension, and the cable channel material [21]. The impact of the cable elongation on the accuracy of the robot control is non-negligible, especially once the cable length is considerably large (>500mm). In addition, the friction along the driving cables also introduces time delay and backlash to the robot control, which slows down the responding speed and decreases the repeatability of the system. Therefore, a sensing approach is needed for slender continuum robots to measure and monitor the cable elongation in real-time for accurate positional controls of the shape of the arm.

In practical work, the multiple-section design even amplifies the effects introduced by the problems discussed above, since the actuation cables of a distal section inevitably pass through a proximal one, these cables always can affect the shape of the proximal section once the tension force varies. This will lead to coupled motions between sections, which challenges the model-based approach of continuum robot control.

Overall, as a trade-off of using the space-saving spool mechanism (rotary actuation), predicting the actual cable lengths is one of the main challenges, which also needs to consider the cable elongation caused by the friction along the cable and the uncertain cable windings. The multiple-section design also introduces the coupling problem, compounding the control challenges. Hence, it is necessary to develop a sensing system to provide feedback on the actual cable displacement at the proximal end of the arm structure. Further, a section-by-section closed-loop control approach with a real-time tip position(s) feedback system is required to improve the control accuracy of multiple-section continuum robots in work-space, when working in complex environments.

To deal with the problems listed above, a new design concept of a hybrid sensing system is proposed, which consists of a dual displacement sensor system that evaluates the errors stemming from the spool cables and a self-carried visual tracking system that tracks the section tips in reference coordinates (i.e., the base of each section, as shown in Fig. 2a).

As illustrated in Fig. 2a, the dual displacement sensor system (⑤) consists of rotary (①) and linear (②) encoders, where the linear encoders measure the real-time cable displacement at the proximal end of the arm, and the rotary encoders indicate the theoretical cable displacement at the motor end. By comparing these two groups of feedback values, the dual displacement sensor system works to evaluate the displacement error in the actuation pack and estimate the cable elongation in the arm

structure according to the ratio of $\frac{\text{displacement error}}{\text{cable length}}$ (more details are in Section III.A). Implemented with a novel two-stage cable displacement control approach, this device can significantly improve the control accuracy in the joint space (will be presented in Section IV.C).

The self-carried visual tracking system (⑥) equips the continuum robot with several paired observe-reference camera & marker arrays (③) grouped by miniature probe cameras and visual markers. These arrays are attached to the base of each section, aiming to detect the position of the section tip relative to the section base (the reference coordinate). A head camera (④) is also attached to the distal tip to observe the external environmental features and accomplish tasks such as obstacle avoidance. This tracking system helps locate the robot tips section-by-section, provides position feedback to the controller, and achieves a closed-loop control in task space.

Integrated with a novel two-level closed-loop controller (Section III), the whole system was validated that it can successfully compensate for the control error in both joint space (cable-displacement) and work-space (tip-positioning) simultaneously, and significantly improve the control accuracy of a two-section continuum robot (Section IV).

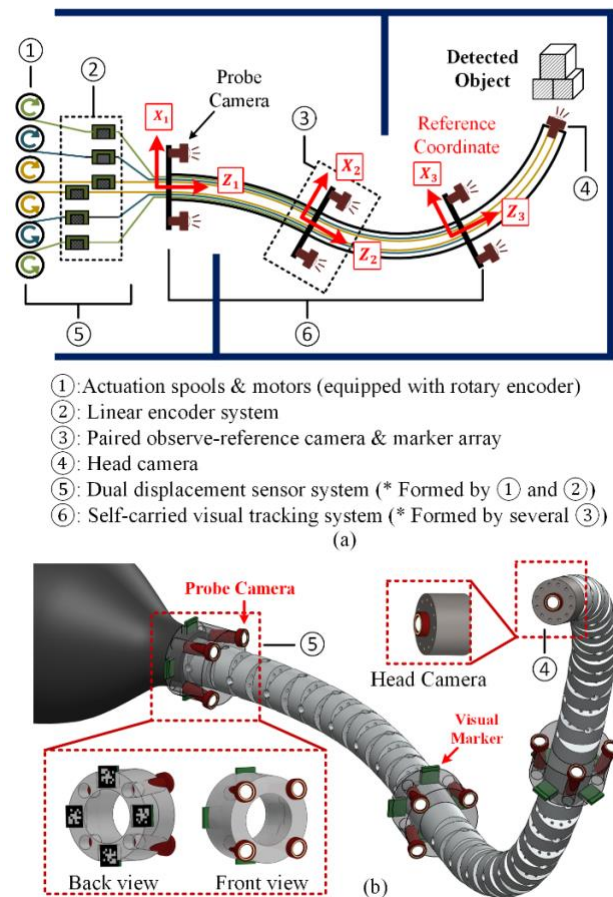


Fig. 2 The concept of a hybrid sensing system. (a) The sensing system is composed of a dual displacement sensor system (linear & rotary encoders) and a self-carried visual tracking system. (b) A 3-D sketch of the self-carried visual tracking system, the probe cameras are fixed on a ring-shaped structure to form a paired observe-reference camera & marker array, tracking the visual marker attached at the backside of a front ring.

III. THE TWO-LEVEL CLOSED-LOOP CONTROLLER BASED ON THE HYBRID SENSING SYSTEM

Precise positional control of continuum robots requires comprehensive feedback regarding the cable displacement and tip-position of each section. This chapter develops a two-level closed-loop control algorithm (Fig. 3), which consists of low-level joint-space control of actuation cable displacements and high-level work-space control of tip positions working in sequence. The joint-space controller is based on a two-stage cable displacement control approach and the feedback from the dual displacement sensor system, aiming to minimize the displacement control error of actuation cables. Correspondingly, the work-space controller relies on the feedback from the self-carried visual tracking system and a novel indirect measurement based tip-adjustment strategy, to accurately position the tip in 3D space (Section III.B). An auxiliary in-process cable tension compensation approach is also implemented. Within this framework, the robot can drive its distal tip to the desired position according to the section-by-section tip tracking, and the in-process tension adjustment approach also keeps the actuation cables appropriately tensioned and efficiently converge the tip errors.

A. The Joint-space cable displacement controller

The main error within the joint space (i.e., the displacement control of the actuation cables) is from the inexact prediction of linear motion raised by unideal cable winding and cable elongation (Fig. 1). This section discusses the implementation of the proposed dual displacement sensor system and a novel two-stage control approach to compensate for these control errors.

1) The dual displacement sensor system

The dual displacement sensor system is composed of the rotary encoders placed at the motor end and the linear encoders embedded between the actuation pack and the arm of a robot (Fig. 2a). The rotary encoder works to indicate the theoretical cable displacement according to motor rotation angles and the linear encoder is supposed to read the real-time cable displacement at the proximal end of the arm when the actuation cables are clamped with the encoder chips. By comparing the reading from the two types of displacement sensors, this system

can precisely measure the cable displacement at the proximal end of the arm and predict the elongation in the arm structure according to known error, which essentially helps to minimize the displacement error of the whole system.

2) The two-stage cable-displacement control approach

In this part, a cable displacement control approach based on the dual displacement sensor system (linear & rotary encoders) is proposed to overcome the drawback of the rotary actuation design (Section II). The core idea of this approach is to divide the actuation cables into active cables and passive cables (Fig. 4a) and use different control strategies to drive these cables, followed by displacement error compensation according to the two types of displacement feedback, as shown in Fig. 4b.

In a continuum robot system, there are two primary control parameters for a constant curvature section, bending angle θ and direction angle φ , the former represents the degree of the arc, and the latter indicates the rotation of the bending plane related to the axis in the arm length direction (reference). When a new command of the desired robot configuration $(\theta, \varphi)_d$ is sent to the robot controller, the theoretical (desired) cable displacement L_d is outputted based on the kinematics model.

In the first-stage control, the value of L_d is converted to motor rotation angle according to the spool parameters (Section II) to drive all the actuation cables monitored by the rotary encoders. Since then, the theoretical cable displacement at the motor end L_{m1} and the actual cable displacement at the robot proximal end L_{l1} can be compared, to investigate the displacement error $(L_{l1} - L_{m1})$ in the actuation pack. As mentioned before, this error comes from the unideal cable winding and elongation. Thus, the elongation error L_e in the arm can be predicted by multiplying the length ratio $\frac{L}{L'}$ with an introduced scale factor k (where L and L' are the nominal cable length in the arm structure and the actuation pack, respectively, when the arm is straight).

The secondary regulation combines the displacement error measured in the actuation pack and the predictive elongation in the arm structure as a new adjustment target L_+ . In this stage, the actuation cables are classified into two groups, active and passive cables. The cable lengths are denoted as L_+ . The active cables have a negative relative displacement (pull cables out of the arm by spools, $L_+ < 0$), while the passive cables have

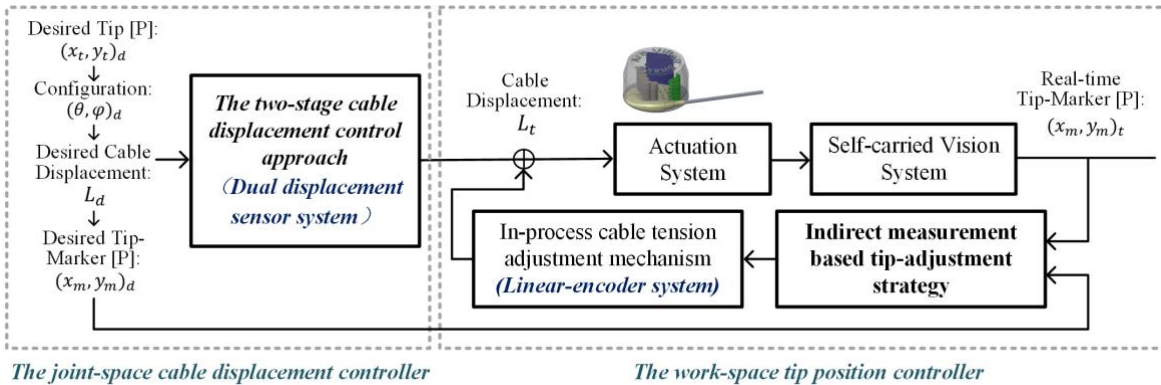


Fig. 3 Control diagram for the two-level closed-loop controller supported by the hybrid sensing system. The joint-space cable displacement control is accomplished by the two-stage cable displacement control approach, based on feedback from the dual displacement sensor system. The work-space tip position control is achieved by the indirect measurement based tip-adjustment strategy, which relies on the section-by-section tip tracking provided by the self-carried visual tracking system.

positive relative displacement, as shown in Fig. 4a. Only the motors connecting with active cables get feedback from the linear encoder for the displacement control in actuation space. The passive cables are controlled by the rotary encoder at the motor end, compensated by $\Delta L = L_d - L_{l2}$ (where L_d is the desired cable displacement and L_{l2} is linear encoder feedback after the second regulation for the passive cables). Finally, the actuation cables reach a displacement of L_t , which is considered as the real-time displacement (i.e., for the driving cables, $L_t = L_d$, for the passive cables, the L_t maybe slightly differ from L_d).

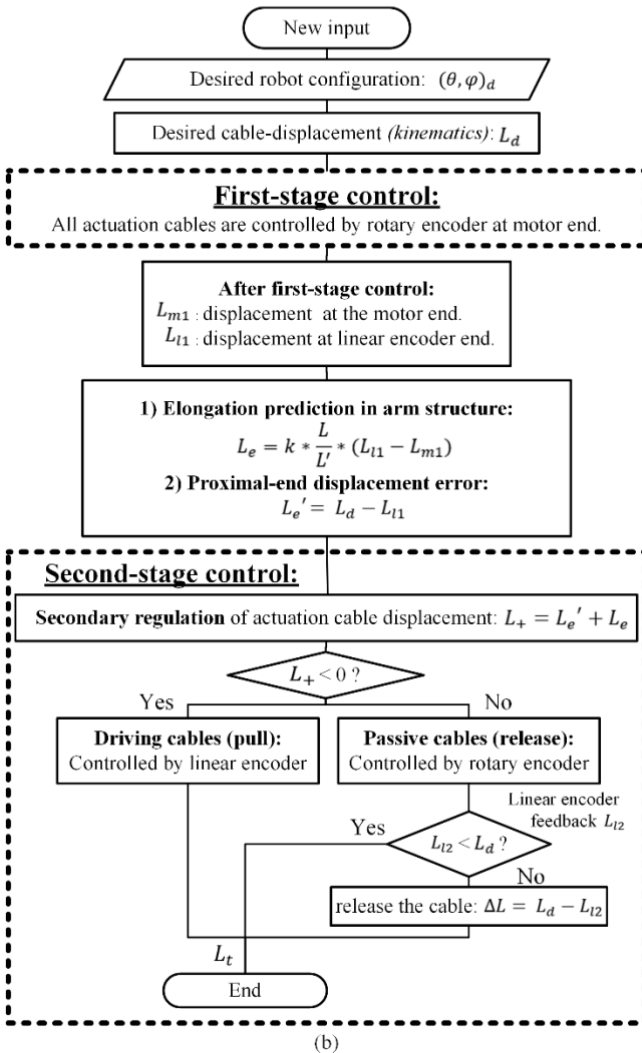
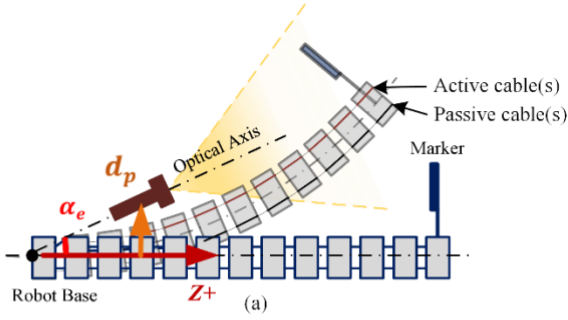


Fig. 4 Joint space cable displacement control. (a) Illustration of a single-section robot with a self-carried camera. The active cable is on

the bending side and the passive cable is on the opposite side. (b) The two-stage cable-displacement control approach is based on linear and rotary encoders measurement. For a specific robot bending angle θ and phase angle φ , the first-stage control drives the cable to an approximate position. The secondary regulation predicts elongation in the arm structure and compensates for the displacement error measured in the actuation pack.

This approach ensures each actuation cable keeps a proper tension and improves control accuracy & efficiency in the joint space, as validated in Section IV.

B. The Work-space Tip Position Controller Based on The Paired Observe-reference Camera & Marker Arrays

The work-space tip position controller works to accurately position the distal tip of a continuum robot in 3D space. Basically, this controller converges the tip errors to control actions by a novel indirect measurement based tip-adjustment strategy, where the tip errors are fed back by the self-carried visual tracking system.

1) Design and Integration of the self-carried visual tracking system

The self-carried visual tracking system is composed of several camera & marker arrays as shown in Fig. 2b). It is designed for section-by-section tip tracking to improve the control accuracy of the arm in the work-space, as discussed in Section II. This part proposes a detailed system specification, including hardware design for the camera & marker arrays and software development for the visual processor.

A **paired observe-reference camera & marker array** is a basic unit of the self-carried visual tracking system, which consists of several forward-looking probe cameras embedded in a 3-d printed ring-shaped structure. Each single-section-arm is equipped with two rings; the front ring fixed on the tip carries several visual markers, and the proximal ring set at the base works to track the corresponding tip-attached marker(s) in the reference coordinates (Fig. 2b). There are two critical parameters for the camera & marker array design, optimal camera elevation angle α_e and optimal spacing d_p (Fig. 4a). The following criteria need to be considered to keep the visual marker in sight of the camera arrays: 1) elevation angle of each camera (α_e) should be as large as possible to extend the total detection area of the camera array (especially when the size of cameras limits the camera-view-angle); 2) an intersection area of FOVs (i.e., the field of view) between adjacent cameras needs to be settled to make sure the objective marker can transit smoothly between different camera views; 3) using a minimal number of cameras to allow a compact design for the camera & marker arrays.

A simple spatial geometric model can be established to describe a single camera-marker array, where the work-space of the robot tip is presented as a circular cone and the visual fields of cameras are presented as rectangular pyramids (Fig. 5a) with fixed vertexes. The elevation angle α_e and optimal spacing d_p can be found by iteratively adjusting the angle between the rectangular pyramid and circular cone until the criteria are satisfied. For the selected camera on this prototype robot, the optimal camera elevation angle is 18 degrees with four probe cameras needed on each array; the maximum detectable bending of a single-section-arm is 66.7 degrees.

When the bending angle of the arm exceeds the maximum detectable area, the robot will run under an open-loop mode, with no measurement and compensation of tip-positioning error, until the tip(s) are visible again. In the following experiments, a bending angle limit was implemented on the robot controller to avoid overbending.

The visual processor processes the feedback images and outputs the position of the target markers in the reference coordinate, which is developed based on the MATLAB computer vision toolbox and OpenCV library. The whole process includes calibration and marker tracking. Calibration can figure out the intrinsic & extrinsic parameters of the visual system, as well as the geometrical relation between camera coordinate and reference coordinate (Fig. 5a). These parameters are used to convert the 2D measurement from cameras (2-D pixel images of detected markers) to 3D position in the real world. Further, the section-by-section tip-tracking is based on the OpenCV library of ArUco marker detection [22], which is a single-marker-based visual tracking method enabling a compact design of paired camera-marker arrays. Under this work frame, each camera is assigned to a specific marker array with unique patterns and ID numbers, to obviate the interferences from mismatching (between markers & cameras) and other obstacles. To avoid the effects of camera blur and vibration, a camera-reading filter is also implemented in the tracking processor, which deletes abnormal readings and takes an average for valid results, making the measurement more feasible.

2) The indirect measurement based tip-adjustment strategy.

The indirect measurement based tip-adjustment strategy is a method that convert marker error vectors to cable-displacement adjustment value, aiming to correct tip position gradually.

As mentioned previously, this method doesn't track the exact position of the robot tip but employs the positional measurement of a tip-attached marker as feedback (Fig. 5a). Detailly, as shown in Fig. 3, when the desired tip position $(x_t, y_t)_d$ is defined in the reference coordinate of each section, the desired robot configuration $(\theta, \varphi)_d$ (arc parameters), the desired actuation cable displacement L_d , and the desired position of tip-attached marker $(x_m, y_m)_d$ are calculated according to the kinematics. The actuation cables are firstly driven by the joint-space controller (Section III.A) to achieve displacement of L_t . Once the robot reacts and the real-time position feedback of the tip-attached marker $(x_m, y_m)_t$ is fed back by the camera arrays, the work-space tip position controller is triggered. The Cartesian positional error vector of the marker $\vec{E}_m \in R^2$ (i.e., the error between desired & actual marker position, as shown in Fig. 5b) is treated as tip error vector² and used to calculate the cable-displacement adjustment value $\Delta L'_t$, gradually drive the distal tip to the desired point $(x_t, y_t)_d$.

To substitute the exact tip error by measured marker error, this tip-adjustment strategy is developed based on the following

two assumptions: 1) The actual tip-position is close to the desired tip-position; 2) The positional error vector at the actual section tip (\vec{E}_t) are equivalent to the positional error vector at the tip-attached marker (\vec{E}_m).

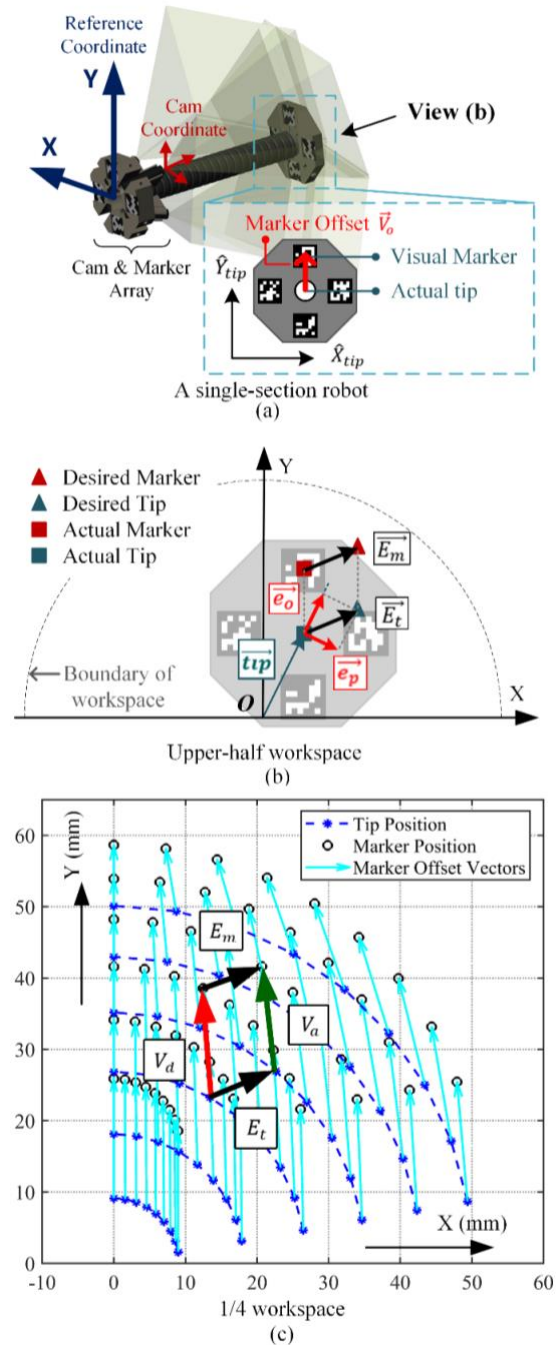


Fig. 5 Explanation for the indirect measurement based tip-adjustment strategy. (a) A single-section continuum robot. (b) A front view of the robot work-space (projection view), which explains the principle of error decomposition in polar coordinate. Point o is the center of the workspace (i.e., start point of a robot tip when the arm is straight), \vec{E}_m

² Theoretically, since the visual markers are fixed on robot tips with known relative position, the exact tip position could be calculated from measured marker position and orientation. However, limited by the marker size, the orientation measurement of the visual marker was not employed since its deviation is non-negligible near the singularity point (when the

bending angle is small). Therefore, only the positional vector $\in R^3$ of the visual marker was received by the robot controller to calculate positioning error of markers and substitute for tip error vectors, which can also guarantee the feedback rate.

and \vec{E}_t are the positioning error of the visual marker and robot tip, \vec{e}_o and \vec{e}_p are the error components. (c) marker offset vectors in $1/4$ workspace (the blue dots represent robot tip position, and the black circles represent visual marker position).

According to the forward kinematics, the orientation of the section tip R_{tip} refer to the reference coordinate of each section can be expressed as [14]:

$$R_{tip} = [\hat{X}_{tip} \ \hat{Y}_{tip} \ \hat{Z}_{tip}] \quad (1)$$

$$= Rot_z(\varphi) * Rot_y(\theta) * Rot_z(-\varphi)$$

Where $Rot_K(\varphi)$ denotes to rotation operator which performs a rotation about the axis \vec{K} of a reference coordinate by φ degrees; φ and θ represent the direction and bending angle of the section.

Calculated from equation (1), the unit vectors giving the principal directions of the tip coordinate \hat{X}_{tip} and \hat{Y}_{tip} (Fig. 5a) can be formulated as:

$$\hat{X}_{tip} = \begin{bmatrix} (\sin\varphi)^2 + (\cos\varphi)^2 * \cos\theta \\ \cos\varphi * \cos\theta * \sin\varphi - \cos\varphi * \sin\varphi \\ -\cos\varphi * \sin\theta \end{bmatrix} \quad (2)$$

$$\hat{Y}_{tip} = \begin{bmatrix} \cos\varphi * \cos\theta * \sin\varphi - \cos\varphi * \sin\varphi \\ (\cos\varphi)^2 + \cos\theta * \sin\varphi^2 \\ -\sin\varphi * \sin\theta \end{bmatrix} \quad (3)$$

Thus, the vector denoting marker offset \vec{V}_o (Fig. 5a & c) has the form of:

$$\vec{V}_o = A \cdot \hat{X}_{tip} + B \cdot \hat{Y}_{tip} = [V_{o(x)} \ V_{o(y)} \ V_{o(z)}]^T \quad (4)$$

Where A and B are coefficients to determine the direction of the marker offset \vec{V}_o (when the marker is on the y axis as shown in Fig. 5a, A = 0, B = 1).

Projected to the X-Y plane, $\vec{V}_{o(xy)}$ can be written as:

$$\vec{V}_{o(xy)} = [V_{o(x)} \ V_{o(y)}]^T \quad (5)$$

$$V_{o(x)} = A\{(\sin\varphi)^2 + (\cos\varphi)^2 * \cos\theta\} + B\{\cos\varphi * \cos\theta * \sin\varphi - \cos\varphi * \sin\varphi\}$$

$$V_{o(y)} = A\{\cos\varphi * \cos\theta * \sin\varphi - \cos\varphi * \sin\varphi\} + B\{(\cos\varphi)^2 + \cos\theta * \sin\varphi^2\}$$

To model the tip-approaching process, assume the tip is expected to achieve a target position (θ_d, φ_d) from current position (θ_a, φ_a) (Fig. 5b-c), where $\theta_d = \theta_a + \Delta\theta$ and $\varphi_d = \varphi_a + \Delta\varphi$. The marker offset vectors are denoted as \vec{V}_a and \vec{V}_d , respectively (Fig. 5c):

$$\vec{V}_a = \vec{V}_{o(xy)}(\theta_a, \varphi_a) \quad (6)$$

$$\vec{V}_d = \vec{V}_{o(xy)}(\theta_a + \Delta\theta, \varphi_a + \Delta\varphi) \quad (7)$$

In the current working space of bending angle $\theta_a \in [0, \frac{\pi}{3}]$, direction angle $\varphi_a \in [0, 2\pi]$, when $(\Delta\theta, \Delta\varphi) \leq 3^\circ$, \vec{V}_a and \vec{V}_d has a maximum angular difference of 2.17 degrees and a maximum modular difference of 0.49 mm, which allows the \vec{V}_a and \vec{V}_d to be treated as parallel and equal vectors, thus \vec{E}_m and \vec{E}_t can also be seen as equivalent vectors. As the tip approaches the target point, the difference between \vec{E}_m and \vec{E}_t will be even smaller

(Fig. 5c). Therefore, the tip error vector of the section \vec{E}_t can be replaced by the marker error vector \vec{E}_m , and measured by the self-carried visual tracking system (comparing the desired & feedbacked marker position) due to the similarity.

To figure out the control action of $\Delta\theta$ and $\Delta\varphi$ (i.e., the adjustment values of robot configuration), the tip error \vec{E}_t is firstly decomposed in polar coordinate along the direction of the tip vector \vec{tip} into orthogonal components \vec{e}_o and \vec{e}_p (Fig. 5b), and convert to $\Delta\theta$ and $\Delta\varphi$ according to following rules:

$$\Delta\theta = |\vec{e}_o| * (k_1 + k_1') \quad (8)$$

k_1 and k_1' are the coefficients defined as:

$$k_1 = \frac{d(|\vec{tip}|)}{d(\theta_d)} = \frac{L}{\theta_d} (1 - \cos\theta_d)$$

$$k_1' \propto \left[\frac{d(|\vec{e}_{o_{i-n}}|, \dots, |\vec{e}_{o_{i-1}}|, |\vec{e}_{o_i}|)}{di} \right]^{-1}$$

$$\Delta\varphi = |\vec{e}_p| * (k_2 + k_2') \quad (9)$$

k_2 and k_2' are the coefficients defined as:

$$k_2 = \frac{|\vec{e}_p|}{|\vec{tip}|}$$

$$k_2' \propto \left[\frac{d(|\vec{e}_{p_{i-n}}|, \dots, |\vec{e}_{p_{i-1}}|, |\vec{e}_{p_i}|)}{di} \right]^{-1}$$

Where $(k_1 + k_1')$ and $(k_2 + k_2')$ are the equivalent proportional gain for \vec{e}_o and \vec{e}_p , respectively. k_1 and k_2 are calculated from kinematics. k_1' and k_2' are relative to the convergence rate of tip error, i is the iteration number.

Finally, the cable-displacement adjustment $\Delta L'_t$ can be calculated from $(\Delta\theta, \Delta\varphi)$ via kinematics and applied to correct tip-position errors.

The tip adjustment process is terminated after all the section(s) achieved the desired control tolerance in their reference coordinates. The experiment data was presented in the reference coordinate and global coordinate to evaluate the performance of the robot in Section IV.

3) The in-process cable tension correction approach

Additionally, within the framework of the controller, the cable tension is supervised by comparing the rotary encoder reading at the motor end and the linear encoder reading at the proximal end of the robot arm. As Fig. 3 shows, once the cable slack is detected (i.e. reading of rotary encoder L_m is larger than Linear encoder reading L_l), the controller will give an extra negative displacement adjustment $\Delta L_{comp} = k_c \times (L_l - L_m)$ to the corresponding actuation cable(s), to keep the cable in tension, where k_c is the compensation coefficient ranges within (0, 1).

Overall, the indirect measurement based tip-adjustment strategy expands the sensing ability of a continuum robot system as well as saving computational resource. Cooperating with the dual displacement sensor system and the self-carried visual tracking system, the two-level closed-loop controller can converge the robot tip(s) to desired position in local work-spaces efficiently, which largely improves the controllability.

IV. EXPERIMENT & RESULTS

This section presents a series of experiments to validate the hybrid sensing system on a two-section continuum robot with 4 degree-of-freedom, as an example of a multiple-section system. Firstly, the dual displacement sensor system and self-carried visual tracking systems are tested separately to evaluate sensing feasibility. Then, the synergetic sensing algorithm is integrated into the proposed closed-loop controller in task space to investigate the tip-positioning performance of this robot.

A. The Continuum Robot System

The robot is a two-section tendon-driven continuum arm, as demonstrated in Fig. 6a. Each active section contains 20 disks with a section length of 120 mm, actuated by three steel cables. The robot employs a design of rotary actuation, all the actuation cables are coiled on the spools and then connected to the actuation motors. These motors are inherently equipped with rotary encoders (resolution: 0.09° , Fig. 2, ①) to feedback rotation angle and predict tendon-displacement in conventional kinematics-based open-loop control, which introduces several challenges for controlling as discussed in Section II.

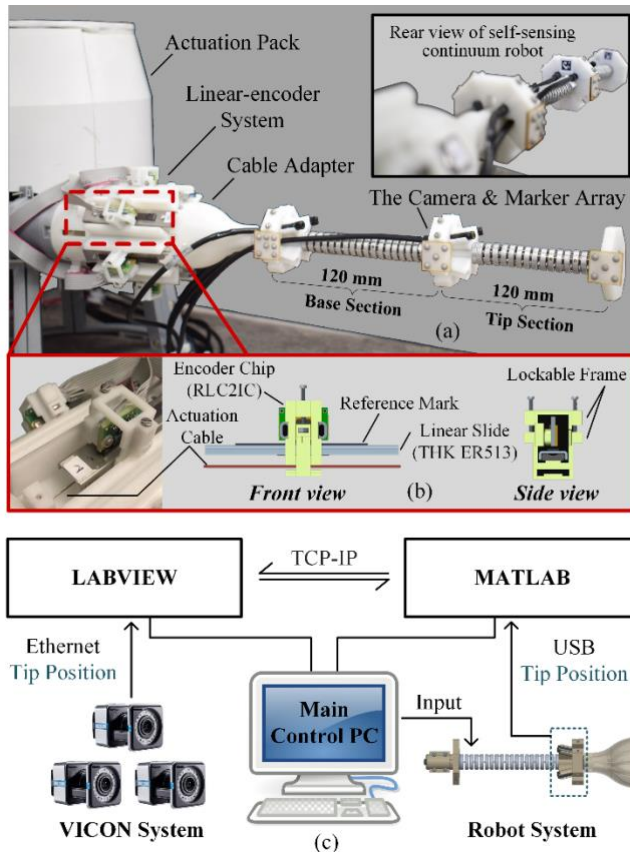


Fig. 6 System overview. (a) the two-section continuum robot with the hybrid sensing system: the linear-encoder system is embedded at the proximal end of the arm, while the camera & marker arrays are fixed at the base of each section. (b) a measurement unit of the linear-encoder system, the actuation cables are clamped by the lockable frame where the encoder chip is attached. (c) System communication: both the robot system and the visual tracking system are controlled by the main PC through LABVIEW and MATLAB separately, and a two-way transport is established via TCP-IP between the two modules; an off-the-shelf position tracking system (VICON) runs on a separate

computer and sends data to the main PC via Ethernet to provide reference data for tip-position.

Fig. 6 a-b demonstrates the proposed hybrid sensing system implemented on the robot. Within the dual displacement sensor system, the linear encoders are mounted at the proximal end of the arm structure, grouped by some measurement units assembled on a 3-D printed structure. Each measurement unit comprises a linear encoder chip (RLC2IC read head, resolution: $2 \mu\text{m}$), a magnetic reference track, and a linear slide (THK ER513), which can clamp with actuation cables to read the displacement value and compare with readings from rotary encoders. The self-carried visual tracking system is formed by several camera & marker arrays attached along with the arm, for section-by-section tip tracking. Some 3-D printed rings work to fix the miniaturized probe cameras (USB inspection cameras with 640×480 pixels resolution) with the section base (reference coordinate), which ensures the feasibility of the visual tracking. The whole robot is controlled by a SbRio9627 FPGA programmed in LABVIEW, and the visual processor (OpenCV) is compiled in MATLAB, communicating with the central controller via TCP-IP (Fig. 6c). The maximum diameter of the robot arm is 45mm, which allows the robot to access some narrow or confined spaces with barrier-free environments to complete some tasks such as inspection and detection.

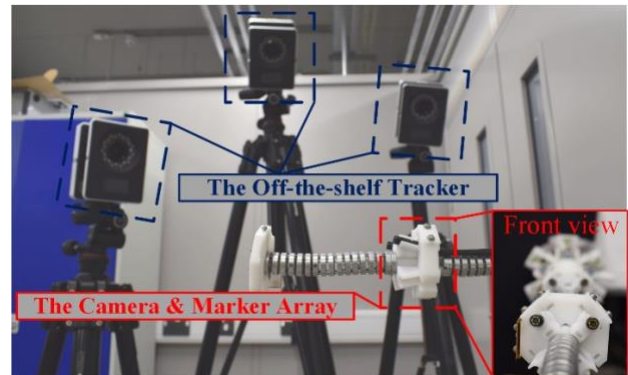


Fig. 7 Experiment Setup: the off-the-shelf tracking system.

During the experiments, an off-the-shelf position tracking system, VICON (Fig. 7), is set aside to track the section tips in the world coordinate, aiming to evaluate the measurement accuracy of the self-carried visual tracking system (in experiment B) and the tip-positioning performance of the robot (in experiment C).

B. Measurement accuracy test for the self-carried visual tracking system

This experiment aimed to evaluate the measurement accuracy of the proposed camera & marker array within the work-space of a single-section arm. Some sampling points are defined along a pre-planned path in the x-y plane of the robot work-space (Fig. 8). The robot arm is commanded to follow the path step-by-step and collect the measurements of the section tip from the off-the-shelf position tracker (VICON) and the proposed self-carried visual tracking system simultaneously. The position data feedbacked by VICON was regarded as the reference value.

Fig. 8 compares the tip-recording from the VICON tracker (blue dot line) and the camera & marker array (red dot line) in

> TMECH-07-2022-13965.R1 <

the trial. The results show that the position measurement from the two sensing systems is consistent along the path, although the difference is slightly more prominent in the center area since it is the intersection area of two adjacent probe cameras.

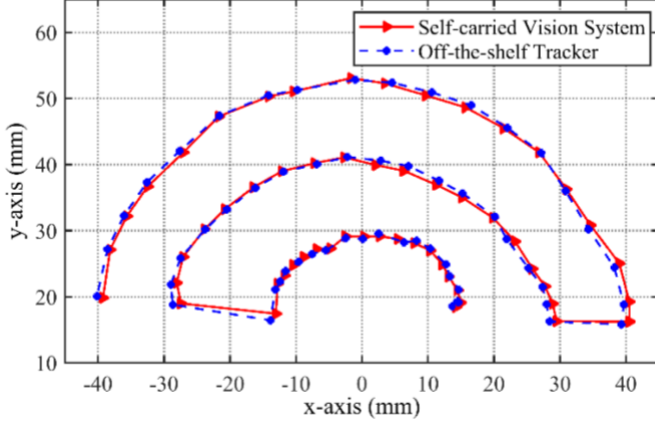


Fig. 8 Tip-tracking performance. Tip trajectories recorded by the off-the-shelf tracker (blue) and camera & marker array (red) are compared for benchmarking the accuracy of the vision system integrated on the continuum arm.

TABLE 1

MEASUREMENT ACCURACY OF THE SELF-CARRIED VISUAL TRACKING SYSTEM COMPARED WITH THE OFF-THE-SHELF POSITION TRACKER (THE VICON SYSTEM)

Min Error (mm)	Max Error	Mean Error	RMSE	Feedback rate
0.09	1.50	0.67	0.36	3Hz

TABLE 1 plots the measurement error of the vision system contrasted to the VICON Tracker. Within the 57-step trail, the mean tracking error is 0.67 mm, and the RMSE is 0.36 mm, with a feedback rate of 3Hz. Overall, the vision system provides feasible tip-position feedback for a single-section arm with the detectable range of the camera & marker array and feedback

rate to achieve closed-loop control in the actual working scenario.

C. Validation for the dual displacement sensor system based two-stage cable displacement control approach

The second experiment has two main objectives: 1) evaluating the cable-displacement control uncertainty introduced by the rotary actuation design (i.e., unideal cable winding and cable elongation); 2) examining the control performance of the new joint-space controller by comparing the tip-positioning accuracy of a 110 mm-long single-section arm under 2 types of controllers (i.e., the conventional kinematics-based open-loop controller relying on the rotary encoders and the new joint-space controller based on the dual displacement sensor system).

A butterfly path is pre-planned for the robot arm with 31 sampling points (Fig. 9d). In the first part of this experiment, the conventional model-based controller is employed, all the actuation cables were controlled by the rotary encoders at the motor end. Meanwhile, the linear encoders measured the actual cable displacement at the proximal end of the arm (Fig. 9a). Fig. 9b illustrated the cable distribution of the tested section, and Fig. 9c compares the theoretical vs actual displacements of each actuation cable in the motion. The results show a clear pattern of cable backlash (i.e., when the driving motors reverse) and elongation (i.e., the displacement error increases as desired displacement increases). Furthermore, the passive cables with positive displacement (opposite to bending side, Fig. 5a) always have more significant control error than active cables with negative displacement (on the bending side) since the friction along with the arm structure, bringing further effect in tip-positioning accuracy.

The second part of this experiment aims to assess the joint-space cable-displacement controller (Section III) by comparing it with the conventional kinematics-based open-loop controller regarding tip-positioning accuracy. The robot would repeat the same motion along the pre-planned path several times, and the

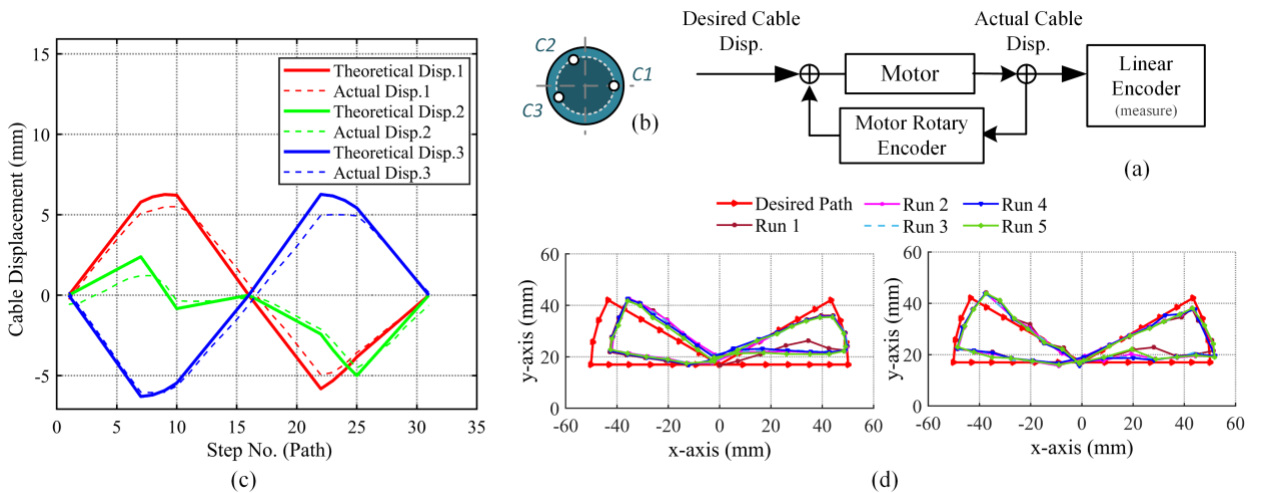


Fig. 9 Validation for the linear encoder system. (a) workflow diagram for experiment C, all actuation cables are controlled by the rotary encoder at the motor end and the linear-encoder system works as measurement device. (b) cable distribution for the tested section; (c) comparison between theoretical cable displacement (solid line) vs actual cable displacement (dot line), which indicates the cable displacement error within the actuation pack. (d) Control performance comparison of the single-section robot between conventional method based of rotary encoder (left figure) and the two-stage cable displacement control approach (right figure).

self-carried visual tracking system provided tip-recording simultaneously. Fig. 9d plots the tip trajectories of the single-section arm with the conventional controller (left figure) and the new joint-space controller (right figure). The displacement error compensator at the proximal end greatly improves the performance of this robot referring to tip accuracy and repeatability. Compared with the open-loop rotary actuation mechanism, the maximum positioning error decreases from 9.96 mm to 6.70 mm, and the mean error decreases from 5.79 mm to 3.13 mm in the x-y plane.

D. Validation for the two-level closed-loop controller with the feedback from the hybrid sensing system

This experiment examines the two-level closed-loop controller with the hybrid sensing feedback, where the robot tip is positioned by the indirect measurement based tip-adjustment strategy. As described in Section III, this controller aims to minimize the tip-positioning error of each section in its reference coordinate. Similar to the previous tests, a continued pre-planned path is given to the robot to mimic the real working scenario like crack detection, metal welding, etc. As illustrated in Fig. 10, the base section is expected to finish a circle path while the tip section will follow a cross-shaped path in their reference coordinates. Eventually, with the synchronous motion of the two sections, the distal tip of the robot will move in a quadrate path in the world coordinate. In this experiment, the control tolerance was set as 0.8 mm. The self-carried visual tracking system and a VICON Tracker recorded tip trajectory simultaneously to monitor control accuracy in local and world coordinates separately.

TABLE 2

TIP-POSITIONING ERROR FOR THE TWO-SECTION ROBOT IN THE REFERENCE COORDINATE

error (mm)	Closed-loop error		Open-loop error	
	mean	max	mean	max
Base Sec	0.38	0.77	1.36	3.00
Tip Sec	0.59	0.80	2.23	5.77

As shown in Fig. 10a and TABLE 2, both sections converged their tip error successfully to the desired control tolerance. The base section performs better than the tip section since its cables have no coupling problem (i.e., the cable control accuracy of a distal section was affected by the proximal section). Compared with conventional PCC-based open-loop control, the proposed closed-loop controller decreased tip-positioning error from 1.36 mm to 0.38 mm for the base section averagely and reduced error by 1.64 mm for the tip section.

TABLE 3

TIP-POSITIONING ERROR FOR THE TWO-SECTION ROBOT IN THE WORLD COORDINATE

Mean error (mm)	Closed-loop error	Open-loop error
Base Sec	0.92	2.43
Tip Sec	1.72	6.50

Fig. 10b and Table 3 demonstrate the control accuracy in world coordinate monitored by the VICON tracker. Since the controller was designed for the reference coordinate operation

(thus, the control tolerances were also set in reference coordinates), the global errors were more extensive than local errors. However, the error is still significantly compensated compared with the open-loop condition, e.g., the mean tip-positioning error was reduced by 1.51 mm and 4.78 mm for the base and tip sections, respectively.

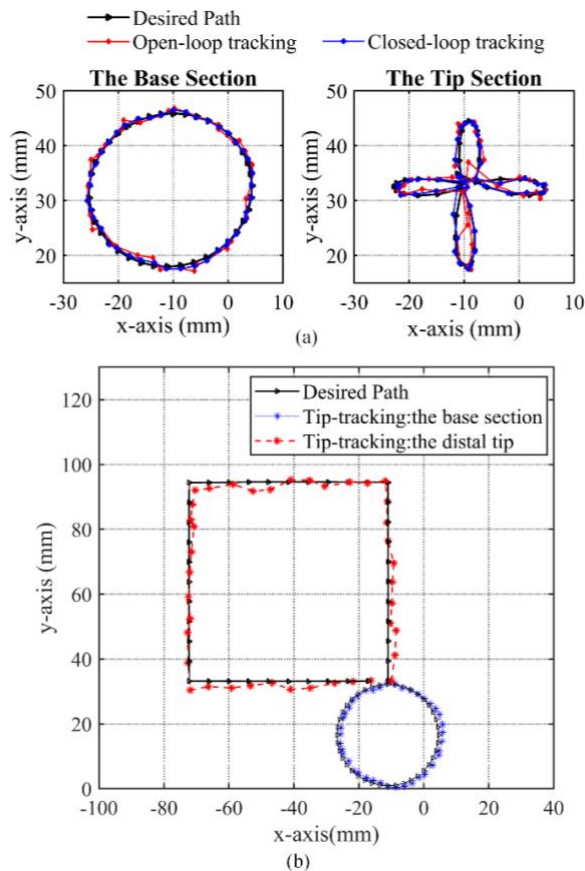


Fig. 10 Tip-positioning performance of the two-level closed-loop controller. a) open-loop & closed-loop control accuracy comparison in the reference coordinate for both sections; b) control accuracy of the distal tip under closed-loop control supported by the hybrid sensing system in the world coordinate (black: desired path; red: the actual path of the distal tip; blue: the actual path of the base-section-tip).

To sum up, the above experiments validated the hybrid sensing system as well as the two-level closed-loop controller, which improves the controllability of a multi-section continuum robot and decreases distal tip error from 6.50 mm to 1.72 mm on average, in the world coordinate. Currently, the robot achieves a great tip-positioning accuracy (point-to-point) with the proposed sensing system and the new controller. The performance can be further enhanced if applying the controller to a robot system with force sensing that keeps cable tension in an ideal range.

V. CONCLUSION

This paper introduces a new hybrid sensing system including a dual displacement sensor system embedded in the actuation pack that employs rotary & linear encoders, and a self-carried visual tracking system integrated along the arm. The camera & marker arrays and linear encoders provide feasible feedback to the robot system, including real-time tip position of each

section and cable displacement at the proximal end of the arm, reducing the errors caused by the rotary actuation (i.e., the spooling) and cable elongation and enabling precise positional control for the system. Furthermore, based on the proposed hybrid sensing system, a novel two-level closed-loop controller is proposed and validated, whose control accuracy was demonstrated both in the joint-space (the two-stage cable displacement control approach) and work-space (the indirect measurement based tip position controller).

It can be found that for a single section arm, the vision system offers tip-tracking with a mean error of 0.67 mm in its workspace. The application of a linear encoder decreases the error of the open-loop control from 5.79 mm to 3.13 mm. Furthermore, under the closed-loop controller, the two-section tip-positioning accuracy of this robot can achieve 1.72 mm when following a pre-planned path.

Further research will explore the application of the self-carried camera arrays and possible improvements to the closed-loop controller. For instance, the head camera at the distal tip can be enrolled in the controller to monitor working environment features and guide the robot in navigation tasks. Modifying the feature-recognition algorithm or considering trajectory error compensation can also improve the control efficiency.

REFERENCES

- [1] T. George Thuruthel, Y. Ansari, E. Falotico, and C. Laschi, "Control Strategies for Soft Robotic Manipulators: A Survey," *Soft Robot*, vol. 5, no. 2, pp. 149-163, Apr 2018, doi: 10.1089/soro.2017.0007.
- [2] A. Melingui, O. Lakkhal, B. Daachi, J. B. Mbede, and R. Merzouki, "Adaptive neural network control of a compact bionic handling arm," *IEEE/ASME Transactions on Mechatronics*, vol. 20, no. 6, pp. 2862-2875, 2015.
- [3] M. Wang, D. Palmer, X. Dong, D. Alatorre, D. Axinte, and A. Norton, "Design and development of a slender dual-structure continuum robot for in-situ aeroengine repair," in *2018 IEEE/RSJ International Conference on Intelligent Robots and Systems (IROS)*, 2018: IEEE, pp. 5648-5653.
- [4] C. G. Frazelle, A. Kapadia, and I. Walker, "Developing a Kinematically Similar Master Device for Extensible Continuum Robot Manipulators," *Journal of Mechanisms and Robotics*, vol. 10, no. 2, 2018, doi: 10.1115/1.4039075.
- [5] W. S. Rone and P. Ben-Tzvi, "Multi-segment continuum robot shape estimation using passive cable displacement," in *2013 IEEE International Symposium on Robotic and Sensors Environments (ROSE)*, 2013: IEEE, pp. 37-42.
- [6] W. Ba, X. Dong, A. Mohammad, M. Wang, D. Axinte, and A. Norton, "Design and validation of a novel fuzzy-logic-based static feedback controller for tendon-driven continuum robots," *IEEE/ASME Transactions on Mechatronics*, 2021.
- [7] S. C. Ryu and P. E. Dupont, "FBG-based shape sensing tubes for continuum robots," in *2014 IEEE International Conference on Robotics and Automation (ICRA)*, 2014: IEEE, pp. 3531-3537.
- [8] G. Gerboni, A. Diodato, G. Ciuti, M. Cianchetti, and A. Menciassi, "Feedback control of soft robot actuators via commercial flex bend sensors," *IEEE/ASME Transactions on Mechatronics*, vol. 22, no. 4, pp. 1881-1888, 2017.
- [9] R. A. Bilodeau, E. L. White, and R. K. Kramer, "Monolithic fabrication of sensors and actuators in a soft robotic gripper," in *2015 IEEE/RSJ International Conference on Intelligent Robots and Systems (IROS)*, 2015: IEEE, pp. 2324-2329.
- [10] A. Bajo, R. E. Goldman, and N. Simaan, "Configuration and joint feedback for enhanced performance of multi-segment continuum robots," in *2011 IEEE International Conference on Robotics and Automation*, 2011: IEEE, pp. 2905-2912.
- [11] NDI. *Electromagnetic Tracking that Supports In-vivo Tool Navigation*. Available: <https://www.ndigital.com/products/3d-guidance/>
- [12] M. C. Yip and D. B. Camarillo, "Model-less feedback control of continuum manipulators in constrained environments," *IEEE Transactions on Robotics*, vol. 30, no. 4, pp. 880-889, 2014.
- [13] W. McMahan, B. A. Jones, and I. D. Walker, "Design and implementation of a multi-section continuum robot: Air-octor," in *2005 IEEE/RSJ International Conference on Intelligent Robots and Systems*, 2005: IEEE, pp. 2578-2585.
- [14] R. J. Webster III and B. A. Jones, "Design and kinematic modeling of constant curvature continuum robots: A review," *The International Journal of Robotics Research*, vol. 29, no. 13, pp. 1661-1683, 2010.
- [15] A. D. Kapadia, K. E. Fry, and I. D. Walker, "Empirical investigation of closed-loop control of extensible continuum manipulators," in *2014 IEEE/RSJ International Conference on Intelligent Robots and Systems*, 2014: IEEE, pp. 329-335.
- [16] D. Braganza, D. M. Dawson, I. D. Walker, and N. Nath, "A neural network controller for continuum robots," *IEEE transactions on robotics*, vol. 23, no. 6, pp. 1270-1277, 2007.
- [17] H. Su, G. Li, D. C. Rucker, R. J. Webster III, and G. S. Fischer, "A concentric tube continuum robot with piezoelectric actuation for MRI-guided closed-loop targeting," *Annals of biomedical engineering*, vol. 44, no. 10, pp. 2863-2873, 2016.
- [18] K.-H. Lee *et al.*, "Nonparametric online learning control for soft continuum robot: An enabling technique for effective endoscopic navigation," *Soft robotics*, vol. 4, no. 4, pp. 324-337, 2017.
- [19] N. Simaan *et al.*, "Design and integration of a telerobotic system for minimally invasive surgery of the throat," *The International journal of robotics research*, vol. 28, no. 9, pp. 1134-1153, 2009.
- [20] D. Axinte *et al.*, "MiRoR—Miniaturized robotic systems for holistic in-situ repair and maintenance works in restrained and hazardous environments," *IEEE/ASME Transactions on Mechatronics*, vol. 23, no. 2, pp. 978-981, 2018.
- [21] T. Kato, I. Okumura, S.-E. Song, A. J. Golby, and N. Hata, "Tendon-driven continuum robot for endoscopic surgery: Preclinical development and validation of a tension propagation model," *IEEE/ASME Transactions on Mechatronics*, vol. 20, no. 5, pp. 2252-2263, 2014.
- [22] OpenCV (2018, Feb. 23). *ArUco Marker Detection*. [Online] Available: https://docs.opencv.org/3.4.1/d9/d6a/group__aruco.html



Yihua. Fang received her B.Eng. degree in Mechanical Engineering from the University of Nottingham, Nottingham, UK, in 2018. She is currently working toward the Ph.D. degree in Robotics, with the Rolls-Royce University Technology Centre (UTC) in Manufacturing and On-wing technology, University of Nottingham. Her research interests include analysis, sensor fusion, and controller development for continuum robots.



Xin Dong received his Ph.D. degree in Mechatronics, Robotics, and Automation Engineering from the University of Nottingham, Nottingham, UK, in 2015. He is currently an Associate Professor working at the University of Nottingham. His research interests are extra slender continuum robots and reconfigurable hexapod robots with novel actuation solutions for application in Aerospace, Nuclear, Oil & Gas, Marine, and rescue.



Abdelkhalick Mohammad received his Ph.D. degree in robotics and mechatronics from Toyohashi University of Technology, Toyohashi, Japan, in 2013. He is currently an Assistant Professor in Mechatronics, at the University of Nottingham, UK. His research interests include mechatronics system design, robotics, machine tool control, and control theory.



Dragos Axinte is Professor of Manufacturing Engineering in the Faculty of Engineering, University of Nottingham. He is Fellow of the Institution of Mechanical Engineer (IMechE) and Fellow of the International Academy of Production Engineering (FCIRP). Since 2009, he is the Director of the Rolls-Royce UTC in Manufacturing and On-Wing Technology. He is also Editor-in-Chief of the International Journal of Machine Tools and Manufacture.